Journal of Alloys and Compounds 509 (2011) 3943–3951

Contents lists available at ScienceDirect

Journal of Alloys and Compounds

journal homepage: www.elsevier.com/locate/jallcom

Studies on morphological and electrical properties of Al incorporated combusted iron oxide

S.S. Shinde, C.H. Bhosale, K.Y. Rajpure*

Electrochemical Materials Laboratory, Department of Physics, Shivaji University, Vidyanagar, Kolhapur 416004, Maharashtra, India

ARTICLE INFO

Article history:
Received 8 December 2010
Received in revised form
23 December 2010
Accepted 25 December 2010
Available online 31 December 2010

Keywords:
Combustion
Iron oxide
Temperature
Morphology
Dielectric and impedance properties

ABSTRACT

The aluminium incorporated iron oxide samples were prepared by combustion route using aluminium nitrate and ferric trichloride as precursors. The samples were characterized for their morphological, dielectrical, impedance and thermal conductivity properties as a function of temperature. A strong low frequency dielectric dispersion is found to exist in these samples; this is ascribed to the presence of the ionized space charge carriers such as oxygen ion vacancies and interfacial polarization. The room temperature dielectric constant and the loss tangent ($\tan\delta$) at 1 kHz are 315 and 0.0855 for optimized 10 at.% Al:Fe_2O_3 sample, respectively. The frequency analysis of dielectric and ac conduction properties of these samples suggests the conduction process in these samples to be via oxygen ion vacancy motion through various defect sites. Impedance spectroscopy is used to characterize the electrical behavior. Results indicate that the relaxation mechanism of the material is temperature and frequency dependent and has dominant bulk contribution in different temperature ranges.

1. Introduction

With the advent of nanotechnology there has been resurge of interest in various transition metal oxides, binary iron oxides such as α-Fe_2O_3, Fe_3O_4 and γ-Fe_2O_3, are the most attractive materials, by virtue of their environmental affinity, abundance and low price. The iron oxide has been the subject of many studies due to their interesting physico-chemical properties. It consists of three main phases according to the chemical valence of Fe ions, i.e. wustite (FeO), which has a rocksalt phase, magnetite (Fe_3O_4) and maghemite (γ-Fe_2O_3), which are both cubic spinel phases, and hematite (α-Fe_2O_3), which is a corundum phase [1]. Hematite and maghemite are of particular interest because of its application in magnetic recording media [2], pigments [3], catalysts [4], solar cells [5] and gas sensitive materials [6]. Maghemite is a metastable phase at ambient conditions, and tends to transform to a stable phase of anti-ferromagnetic hematite (α-Fe_2O_3) when heated above 300 °C [7]. de Resende et al. [8] reported the influence of the borohydride concentration on the composition of the amorphous Fe–B alloy produced by chemical reduction of synthetic, nano-sized iron-oxide particles. They reported the contribution of the $Fe_{1-x}B_x$ phase to the total Mössbauer spectra consisting superposition of a broad sextet and doublet. A study on the preparation of iron aluminium based intermetallic alloy by aluminothermic smelting technique has been investigated by Chakraborty et al. [9]. Rai et al. [10] depict structural and Mössbauer spectroscopic investigation of Fe substituted Ti–Ni shape memory alloys. It is therefore of great interest to deposit the equilibrium anti-ferromagnetic hematite structure. These oxides are dielectric which might be used as capacitors in microelectronic circuits and insulators in active devices such as FET, SFET, and in many other ways. There has been an increasing interest in the study of dielectric and impedance study of oxides as they have been used in microelectronic devices. In comparison to pure α-Fe_2O_3, it has been found that aluminium doped or aluminium modified α-Fe_2O_3 can increase the conductivity to a large extent, which is a basic requirement for its use in high density recording. Besides high conductivity, aluminium doped α-Fe_2O_3 provides improved stability with respect to temperature and stress. The challenge still lies in obtaining doped aluminium into the lattice rather than surface modified iron oxide nanoparticles with high conductivity and low aluminium content for high density magnetic storage materials. The hematite was prepared by various techniques such as chemical co-precipitation, solid state reaction, and combustion. Out of these, the combustion technique is simple, cost effective and easy to prepare the nanoparticles.

We have investigated the preparation and characterization of pure and Al doped iron oxide samples. Influence of Al doping on the morphological, dielectrical and impedance properties has been explored. Also, we studied the dependence of temperature on dielectric properties (dielectric constant, dielectric loss and AC

* Corresponding author. Tel.: +91 231 2609435; fax: +91 231 2691533.
E-mail address: rajpure@yahoo.com (K.Y. Rajpure).

0925-8388/$ – see front matter © 2010 Elsevier B.V. All rights reserved.
doi:10.1016/j.jallcom.2010.12.185

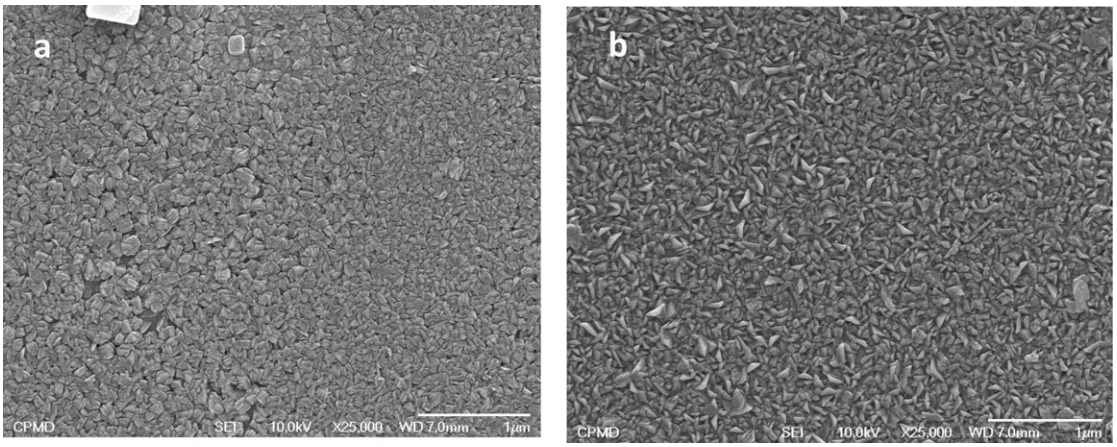

Fig. 1. Scanning electron microscopic images of (a) pure Fe_2O_3 and (b) 10 at.% Al:Fe_2O_3.

conductivity) and impedance analysis. Finally, we have studied the thermal properties viz. specific heat and thermal conductivity.

2. Experimental

The aluminium doped iron oxide samples were prepared by a combustion method using AR grade equimolar (0.1 M) ferric trichloride and aluminium nitrate as precursors. The preparation conditions were carefully controlled. A mixture of precursors in atomic proportion taken in a Pyrex dish, was melted by heating at 80 °C. Glycine was added to the melt and the slurry was introduced into a furnace preheated to 400 °C. After evaporation of the water content, the mixture frothed and ignited to combust with a flame, giving a voluminous and foamy sample. The synthesized powders were annealed at 350 °C. These compositions were further mixed with polyvinyl alcohol as a binder and pressed into pellets of 15 mm diameter and 2–3 mm thickness using a hydraulic press.

The morphological characterization of the samples was observed by using field emission scanning electron microscopy (FE-SEM, Model: JSM-6701F, Japan). The ac parameters such as capacitance (C) and dissipation factor ($\tan\delta$) of the samples were measured in the frequency range 20 Hz to 1 MHz using LCR meter (HP 4284 A). The dielectric constant (ε') was calculated using the relation:

$$\varepsilon' = \frac{C_p t}{\varepsilon_0 A} \quad (1)$$

where C_p is the capacitance of the pellet, t is the thickness of the pellet, A is the area of cross-section of the pellet and ε_0 is the permittivity of free space (8.854×10^{-12} F m^{-1}). The ac conductivity of samples was estimated from the dielectric parameters. As long as the pure charge transport mechanism is the major contributor to the loss mechanisms, the ac conductivity (σ_{AC}) may be calculated using the relation:

$$\sigma_{AC} = \omega\varepsilon'\varepsilon_0 \tan\delta \quad (2)$$

where ω is the angular frequency and $\tan\delta$ is the dissipation factor.

The impedance parameters namely Z' and Z'' for all the samples are measured at various temperatures in the frequency range 20 Hz to 1 MHz using a precision LCR meter bridge (model HP 4284 A). The thermal conductivity was measured by C-T meter made by Teleph Pvt. Ltd., France.

3. Results and discussion

3.1. Morphological analysis

Fig. 1(a) and (b) show the FESEM images of pure and typical 10 at.% aluminium doped iron oxide samples. The micrographs depict the compact and homogeneous distribution of grains with varying sizes. The pure iron oxide sample shows the agglomerated highly dense, compact and homogeneous structure. The large value of the grain size observed by FESEM may be explained by the tendency of small grains to aggregate to big grains in the sample. Apparently, the Al-doping affects the grain size leading to a grain width reduction, as clearly observed in Fig. 1(b). Due to doping compactness of grains and grain size decreases and number of grains increases. Average grain size observed for the pure and 10 at.% aluminium doped iron oxide samples is in the range of 15–55 nm. Therefore, it can be concluded that the morphology and grain size are affected by doping concentration. There are two possibilities associated with the phenomena. One is the effect from outside and the other from inside. It is known that, the oxygen and vapour in the air would have big effect on the morphology. When the exchange of oxygen between grains and air happens, the collapse may happen. We tend to agree with the second mechanism that the collapse is probably due to the strain release of crystallites due to high temperature. The formation of 3D crystallites is mainly governed by surface energy, elastic strain and surface diffusion kinetics.

3.2. Dielectric properties

In most of the solids, the dielectric constant depends on the variation of external factors such as temperature and frequency. The mechanism of dielectric polarization is similar to that of conduction and it has been concluded that the electron exchange interaction results in a local displacement of electrons in the direction of an electric field which determines the polarization [11]. The variation of dielectric constant with frequency of Al doped iron oxide samples at room temperature is shown in Fig. 2. From figure, it is clear that dielectric constant (ε') decreases abruptly at lower frequencies and remains constant at higher frequencies showing dispersion of dielectric constant at lower frequencies. At higher frequencies the dielectric constant remains independent of frequency

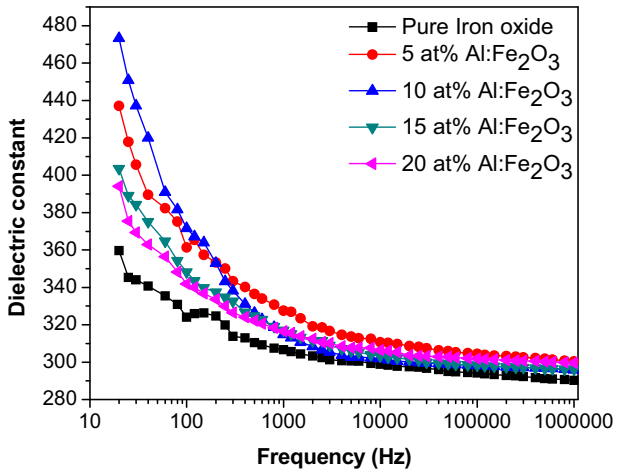

Fig. 2. Variation of room temperature dielectric constant with frequency 0–20 at.% Al:Fe_2O_3 samples.

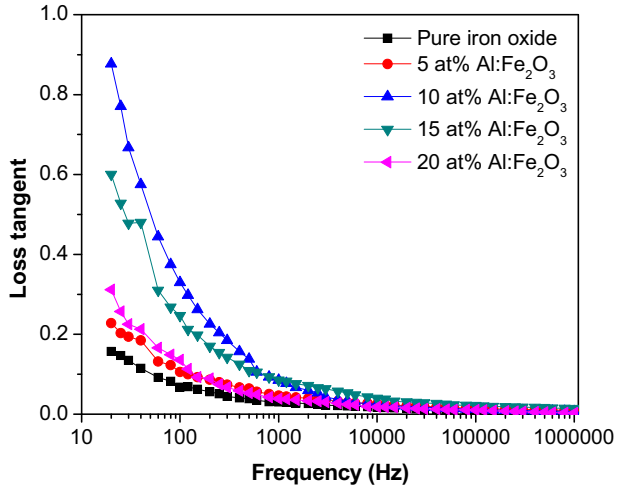

Fig. 3. Variation of loss tangent ($\tan\delta$) with frequency for 0–20 at.% Al:Fe_2O_3 samples.

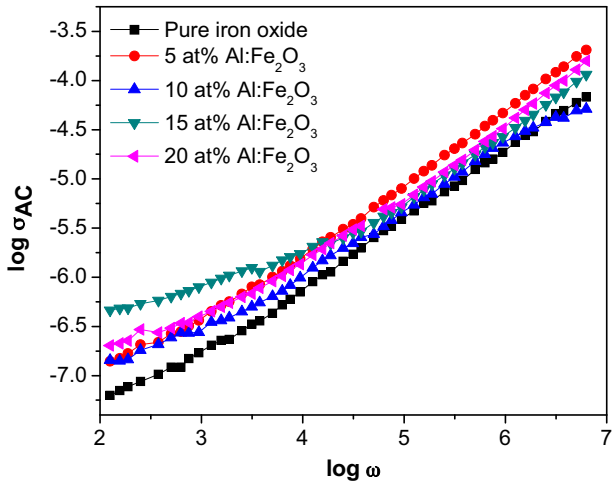

Fig. 4. Variation of ac conductivity with frequency for 0–20 at.% Al:Fe_2O_3 samples.

due to the inability of electric dipoles to follow the fast variation of the alternating applied electric field and accordingly the friction between them will increase. A quantity of heat will thus be generated and internal viscosity of system and hence, dielectric constant will decrease [12]. These frequency independent values are known as static values of the dielectric constant. In composites, the higher value of the dielectric constant at lower frequencies is associated with heterogeneous conduction [13], but sometimes the polaron hopping mechanism results in electronic polarization contributing to low frequency dispersion. This dielectric dispersion is attributed to Maxwell [14] and Wagner [15] type of interfacial polarization in agreement with Koop's phenomenological theory [16]. Since polarization decreases with increasing frequency and reaches constant values, decrease in dielectric constant with frequency is observed. The large value of dielectric constant is associated with space charge polarization and inhomogeneous dielectric structure. These inhomogeneities are impurities, grain structure and pores. The presence of Al^{2+}/Al^{3+} ions gives rise to their displacement in the external electric field direction also contributes to the net polarization.

The variation of dielectric loss with frequency at room temperature is shown in Fig. 3. At lower frequencies $\tan\delta$ is large and it decreases with increasing frequency. The $\tan\delta$ is the energy dissipation in the dielectric system, which is proportional to the imaginary part of dielectric constant. At higher frequencies the losses are reduced and the dipoles contribute to the polarization [17]. The loss factor curve is attributed to domain wall resonance. At higher frequencies, losses are found to be low if, domain wall motion is inhibited and magnetization is forced to change by rotation.

To confirm the conduction mechanism in these composites, the variation of $\log\sigma_{AC}$ with $\log\omega$ was studied (Fig. 4). The plots are observed to be almost linear indicating that the conduction increases with increase in frequency. The linearity of the plots confirms small polaron mechanism of conduction [18–21]. The slight decrease in conductivity is attributed to conduction by mixed polarons. In ionic solids the electrical conductivity is due to the migration of ions and the ionic transport depends on angular frequency. Thus, the ac conductivity (σ_{AC}) is proportional to the angular frequency and it is confirmed here by linear plots of conductivity with angular frequency [22]. Relatively higher value of dielectric constant, loss tangent and ac conductivity in case of the sample prepared at 10 at.% Al doping are observed.

The variation of the dielectric constant with temperature for different Al doping concentrations is shown in Fig. 5. The dielectric data have been obtained in the temperature range (25–275 °C) at 1 kHz frequency. The variation of ε' with temperature explains temperature relaxation phenomena of the material. The dielectric constant increases with increase in temperature showing two maximum values (ε_{max}) at ~60 and 255 °C and then decreases with further increase in temperature. It is observed that the material undergoes a phase transition from microcrystalline to nanocrystalline phase. The first maxima (ε_{max}) is shifted towards lower temperature side (from ~86 to 60) due to Al doping concentration. Basically the charge hopping is a thermally activated process that results in an increase of dielectric polarization proportional to temperature causing an increase in the dielectric constant. The incorporation of the Al in the pure iron oxide lattice dilutes the properties of composites, resulting in reduction of the dielectric constant and broadness of the peak. The dielectric peak broadened over a certain temperature interval indicating the existence of diffuse phase transition. The temperature dependence on dielectric loss of Al doped iron oxide samples is shown Fig. 6. The value of ε'' increases with increasing temperature and loss peak observed at high temperature. The rate of change of ε'' with temperature is very

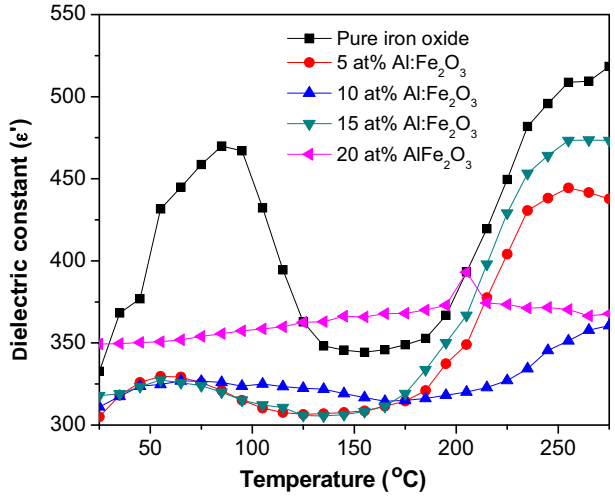

Fig. 5. Variation of dielectric constant with temperature for 0–20 at.% Al:Fe_2O_3 samples.

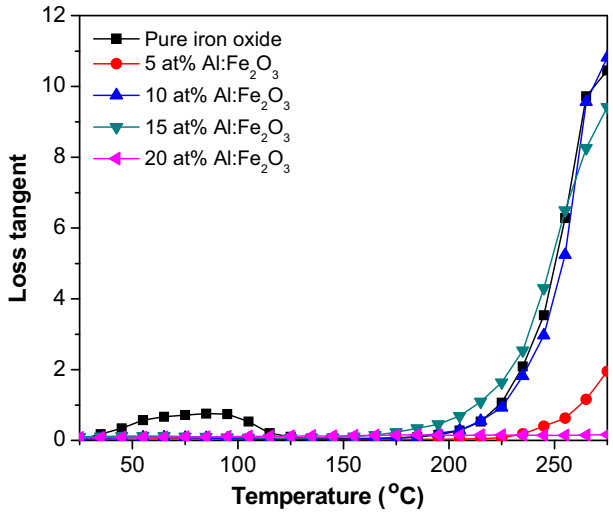

Fig. 6. Variation of loss tangent ($\tan\delta$) with temperature for 0–20 at.% Al:Fe_2O_3 samples.

small (loss almost temperature independent) at lower temperature and sharply increases for higher temperatures. The temperature where this change occurs is approximately 225 °C. The kind of temperature dependence of the ε'' is typically associated with losses by conduction.

3.2.1. Complex impedance spectroscopy

The complex impedance (Z) can be represented as $Z^* = Z' - iZ'' = |Z|\cos\theta - i|Z|\sin\theta$, where Z' and Z'' are the real and imaginary parts of complex impedance, and $|Z|$ and θ are the modulus and complex angle of the complex impedance, respectively. The complex impedance formalism helps to determine interparticle interactions (like grains, grain boundary effects, etc.). Due to the polycrystalline nature of Fe_2O_3, the barrier is modeled as double layer over the grains region. The resistance contributions are generally represented by three parallel circuits (R-C) connected in series and corresponding to the bulk, the grain boundary and the diffusion. Fig. 7(a)–(e) represents the real (Z_r) and imaginary component (Z_i) in the complex plane for different Al doping percentage (0–20 at.%) samples at 50–200 °C temperature. The impedance spectrum is characterized by the appearance of semicircle arcs whose pattern changes, but not its shape, when the temperature is increased. Such pattern tells us about the electrical process occurring within the sample and their correlation with sample microstructure, when modeled in terms of an electrical equivalent circuit [23]. The equivalent circuit configuration for the impedance is $R_g + R_{gb}||C_{gb}$ shown in Fig. 7(f). The intercept with real axis of the semicircle at low frequencies is ascribed to the total resistance RT. On the other hand, the impedance response of grain dominates at high frequencies and the resistances of grain R_g can be deduced from the left intercept of the semicircle with real axis. The intercept of the semicircle with the real axis (Z') at low frequency represents the sum of the resistance of grains and grain boundaries, while the intercept at high frequency represents the resistance of the grains only. Grain boundary resistance decreases with rise in temperature, it seems to the fact that, the grain boundary effect is assisted to lower barrier to the charge carriers motion paving the way for increased electrical transport with rise in temperature. The evidences of grain boundary conduction have been observed in perovskite ceramic, ceramic conductors and also in ceramic dispersed ionically conducting composite polymers. The expression of real (Z') and imaginary (Z'') components of impedance related to the equivalent circuit is:

$$Z' = R_g + \left(\frac{R_{gb}}{1 + R_{gb}^2 C_{gb}^2 \omega^2}\right) \quad (3)$$

$$Z'' = \frac{R_{gb}^2 C_{gb}\omega}{1 + R_{gb}^2 C_{gb}^2 \omega^2} \quad (4)$$

where $\omega = 2\pi f$ and f is the frequency, R_g and C_g are the resistance and capacitance of the grain while R_{gb} and C_{gb} are that of grain boundary. Depending upon the relative rate of decrease of R_g and R_{gb}, and at the same time the relative rate of increase of C_g and C_{gb}, with ω as the variable, the complex impedance curves gradually and successively change from one shape to the other [24], at different temperatures.

As the doping concentration increases the real and imaginary parts of complex impedance decrease up to 10 at.% Al doping concentration (from 10,000 to 1600 KΩ) and then again increase for higher doping concentrations. The one arc is observed for all samples at low frequency representing the sum of resistance of grains and grain boundaries. The impedance value is typically higher at lower temperatures in low-frequency region and decreases gradually with increasing frequency. Also, Z' decreases with increasing temperature indicating an increase in ac conductivity. The value of Z' appears to merge in the high-frequency region irrespective of temperature; this result may possibly be related to release of space charge as a result of reduction in the barrier properties of material with rise in temperature, and may be a responsible factor for the enhancement in conductance of the material with temperature at high frequencies. The values of Z' for all temperatures merge at higher frequencies can be interpreted by the presence of space charge polarization. This interpretation was confirmed by the higher impedance values at lower frequencies.

Polycrystalline materials have variety of frequency dependent effects associated with heterogeneities. One of the advantages of frequency dependent measurements is that the contributions of the bulk material, the grain boundaries and electrode effect can easily be separated, if the time constants associated are different enough [25] to allow separation. The frequency dependent properties of materials can be described via the complex permittivity (ε^*), complex impedance (Z^*) and dielectric loss or dissipation factor ($\tan\delta$). The frequency dependence of Z' is plotted for pure and 10 at.% Al doped iron oxide samples with different temperatures in Fig. 8(a)–(b). The temperature affects strongly the magnitude of resistance. At lower temperatures, Z' decreases monotonically with increasing frequency up to a certain frequency and then becomes frequency independent. At higher temperatures, Z' is almost constant and for even higher frequencies decreases sharply. The higher values of Z' at lower frequencies and low temperatures mean the polarization is larger. The temperatures where this change occurs vary in the material with frequency. This also means that the resistive grain boundaries become conductive at these temperatures. This also shows that the grain boundaries are not relaxing even at very high frequencies even at higher temperatures.

The frequency dependence of Z'' is plotted for pure and 10 at.% Al doped iron oxide samples with different temperatures in Fig. 8(c) and (d). At lower temperatures, Z'' decreases monotonically suggesting that the relaxation is absent. This means that relaxation species are immobile defects and the orientation effects may be associated. The peak shifts towards higher frequency with increasing temperature showing that the resistance of the bulk material is decreasing. Also the magnitude of Z'' decreases with increasing frequency. Figure indicates the spreading of relaxation times. This would imply that, the relaxation is temperature dependent. Thereby relaxation process involved with its discrete relaxation time depending on the temperature. The temperature is increased,

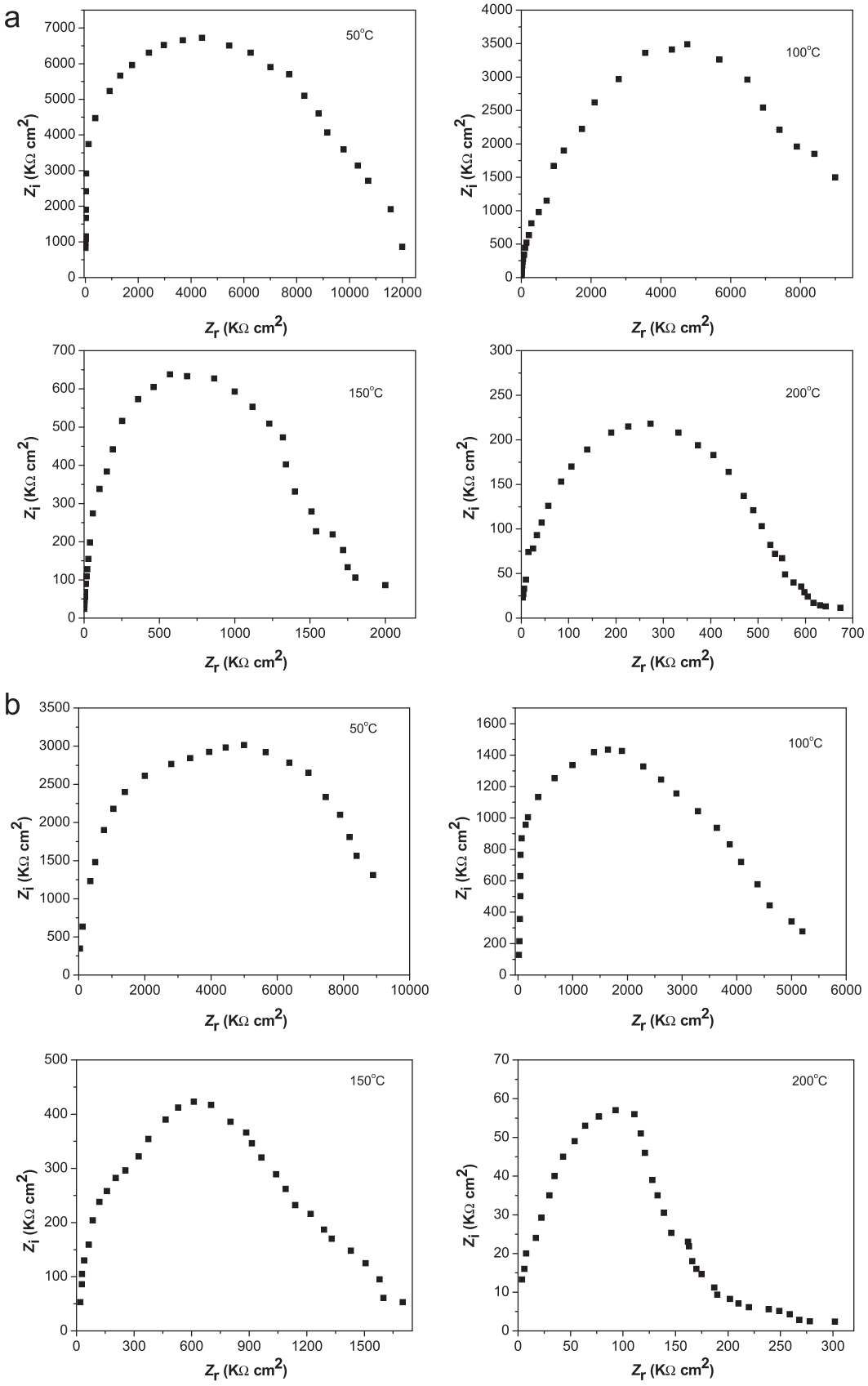

Fig. 7. Complex impedance spectra with temperature for (a) pure Fe_2O_3, (b) 5 at.% Al:Fe_2O_3, (c) 10 at.% Al:Fe_2O_3, (d) 15 at.% Al:Fe_2O_3, (e) 20 at.% Al:Fe_2O_3, (f) electrical equivalent circuit.

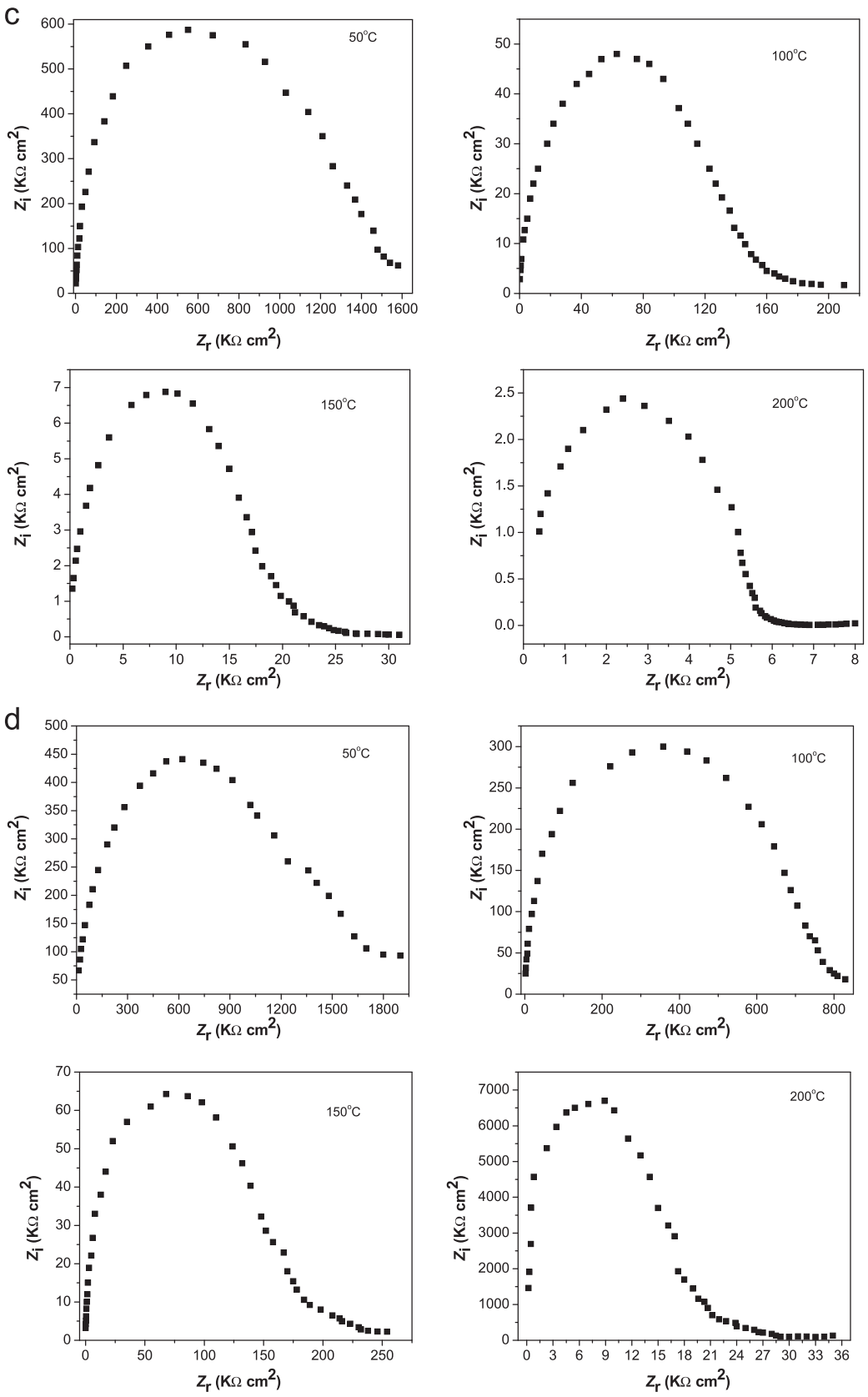

Fig. 7. (*Continued*)

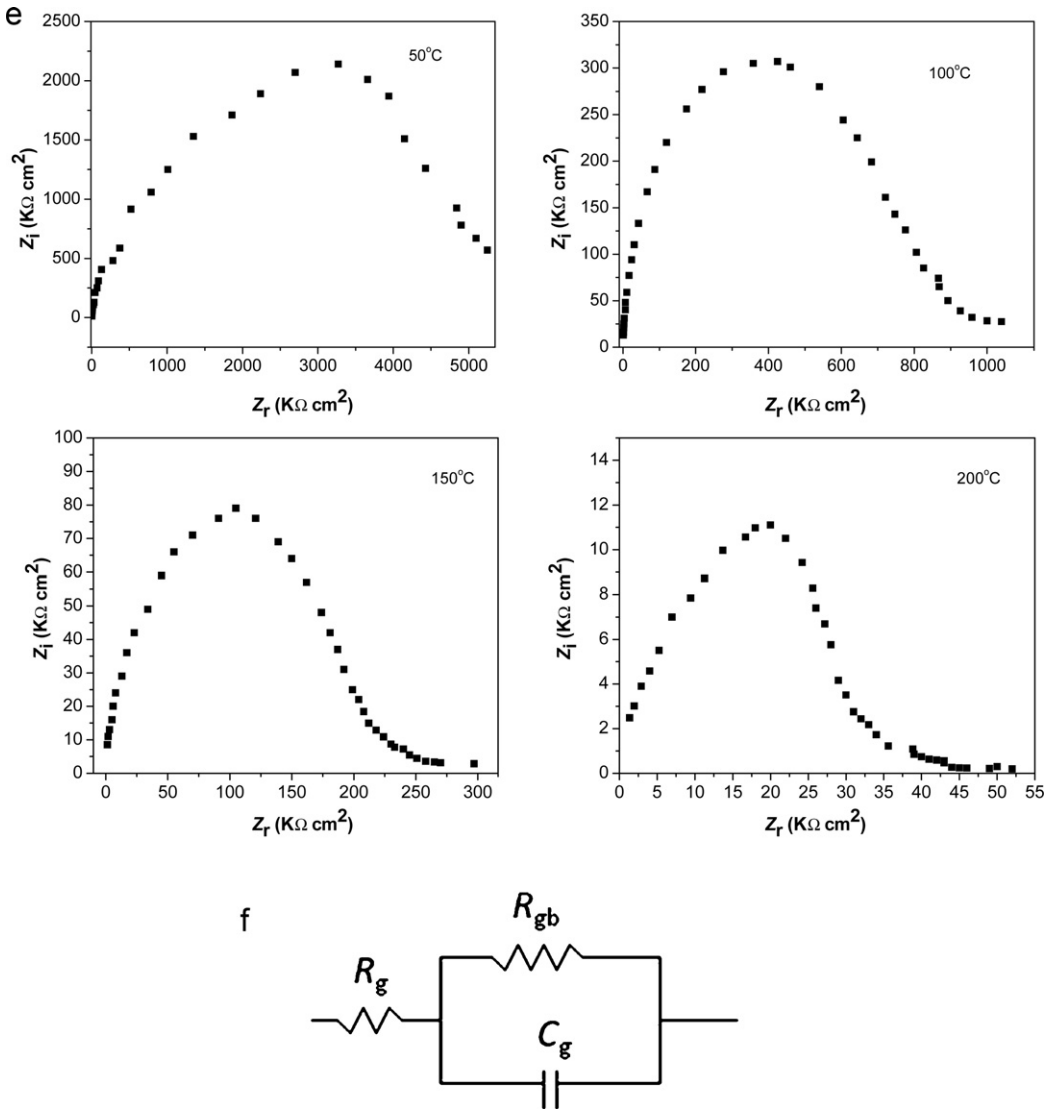

Fig. 7. (*Continued*).

in addition to the expected decrease in magnitude of Z'', there is a shift in the peak frequencies towards the high frequency side. Also, it is evident that with increasing temperature, there is a broadening of peaks at higher temperatures, the curves appear almost flat. This behavior is apparently due to the presence of space charges in the material.

3.3. Thermal conductivity

It is essential to understand the thermo-physical properties of the iron oxide powder samples, when working on those industrial and scientific applications that involve not only equipment design but also analysis, modeling and process control, where there are temperature dependent physical, chemical and biochemical changes. Thermal conductivity analysis is done with the help of the following relation:

$$\Delta T = \frac{RI^2}{L}\frac{1}{4\pi K}[\ln(t) + C] \quad (5)$$

where R is the resistance of the ring probe, K is the thermal conductivity, I is the current, t is the pulse time, L is the length of ring probe, C is the integration constant. The variation of specific heat and thermal conductivity with respect to the doping concentration is illustrated in Fig. 9. Specific heat and thermal conductivity decrease up to 10 at.% Al doping concentration (attains minimum value 845 kJ/m^3 K and 0.369 W/m K respectively) and then increase with higher doping concentrations. The decrease in thermal conductivity means that a phonon conduction behavior is dominant in these powder samples [26], while the increase in thermal conductivity for higher concentrations is mainly attributed to the significant change in microstructure. Apart from contribution of microstructure, the lower thermal conductivity of samples can be attributed to intrinsic factors. The thermal conductivity for crystalline solid is due to change in lattice vibrations, which are usually described in terms of phonons. The expression of the thermal conductivity is derived by Debye described as [27]:

$$k = \frac{1}{3}t_p C_v \nu_m \quad (6)$$

where C_v is the specific heat, ν_m is the phonon velocity and t_p is the mean free path for scattering of phonons. The actual values of thermal conductivity depend sensitively on the defects such as vacancies and solutes which are strong phonon scatterers influencing t_p. The effect of point defects on the phonon mean free path t_p

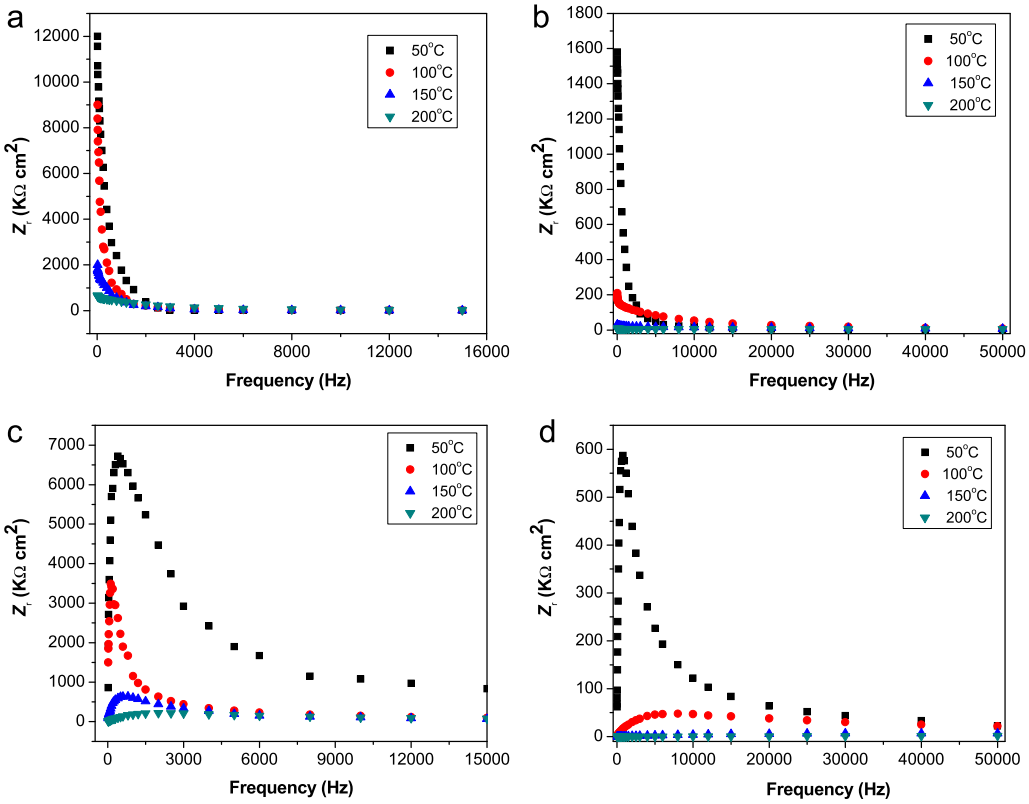

Fig. 8. (a) and (b) Real component of impedance w.r.t. frequency; (c) and (d) imaginary component of impedance w.r.t. frequency for pure and 10 at.% Al:Fe_2O_3 samples at different temperatures.

is given by Klemens [28] as follows:

$$\frac{1}{t_p} = \frac{\alpha^3}{4\pi v^4}\omega^4 c\left(\frac{\Delta M}{M}\right)^2 \quad (7)$$

where α^3 is the volume per atom, v is the transverse wave speed, ω is the phonon frequency, c is the defect concentration per atom, M is the average mass of the host atom, $M + \Delta M$ is the average mass of the solute atom, and for vacancies, the value of $\Delta M/M$ is calculated by:

$$\frac{\Delta M}{M} = \frac{M_\alpha}{2} - 2 \quad (8)$$

where M is the average mass per atom, M_α is the mass of the missing atom, and the term -2 accounts for the potential energy of the missing linkages, or twice the potential energy per atom.

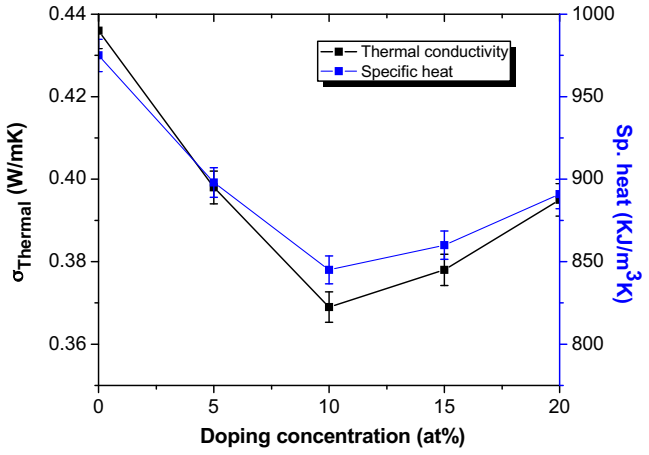

Fig. 9. Variation of thermal conductivity and specific heat with doping concentration at room temperature.

4. Conclusions

The pure and Al doped iron oxide samples were synthesized by combustion route. The micrographs depict the samples are compact and having homogeneously distributed grains with different sizes. The dielectric behavior shows the electronic polarizability at higher frequencies. AC conductivity increases with the increase in the frequency due to hopping mechanism of conduction. The complex impedance reveals that the Z' at low frequencies is due to polarization effect and grain boundaries are non relaxing even at very high frequencies and higher temperatures. Z'' shows distributed relaxation phenomena at high temperatures that are temperature dependent. Frequency dependence of real (ε') and imaginary (ε'') part of the dielectric permittivity shows typical Debye-type dielectric dispersion. The specific heat and thermal conductivity study shows the phonon conduction behavior is dominant in these samples.

Acknowledgement

The authors are very much thankful to Defense Research and Development Organization (DRDO), New Delhi, through its project No. ERIP/ER/0503504/M/01/1007 for the financial support.

References

[1] M.T. Johnson, J.R. Michael, S.R. Gilliss, C.B. Carter, Phil. Mag. A 79 (1999) 2887.
[2] F. Jorgenson, The Complete Handbook of Magnetic Recording, McGraw-Hill, New York, 1996.
[3] F. Jorgenson, J. Mater. Sci. Lett. 12 (1993) 288.
[4] K. Kandori, I. Horii, A. Yasukawa, J. Mater. Sci. 30 (1995) 2145.
[5] J.H. Kennedy, D.J. Dunnwald, Electrochem. Soc. 130 (1983) 2013.

[6] M. Ocana, M.P. Morales, C.J. Serna, J. Colloid Interface Sci. 171 (1995) 85.
[7] X. Ye, D. Lin, Z. Jiao, L. Zhang, J. Phys. D: Appl. Phys. 31 (1998) 2739.
[8] V.G. de Resende, E. De Grave, G.M. da Costa, J. Janssens, J. Alloys Compd. 440 (2007) 236.
[9] S.P. Chakraborty, I.G. Sharma, D.K. Bose, J. Alloys Compd. 280 (1998) 255.
[10] D.K. Rai, T.P. Yadav, V.S. Subrahmanyam, O.N. Srivastava, J. Alloys Compd. 482 (2009) 28.
[11] S.A. Mazen, H.A. Dawoud, Mater. Chem. Phys. 82 (2003) 557.
[12] M.A. Ahmed, S.T. Bishay, G. Abdelatif, J. Phys. Chem. Solids 62 (2001) 1039.
[13] Y. Zhi, A. Chen, J. Appl. Phys. 91 (2002) 794.
[14] J.C. Maxwell, Electricity and Magnetism, Oxford University Press, London, 1993, p. 828.
[15] K.W. Wagner, Ann. Phys. 40 (1993) 818.
[16] C.G. Koop, Phys. Rev. B 83 (1951) 121.
[17] D.C. Agrawal, Asian J. Phys. 6 (1997) 108.
[18] V.S. Sawant, S.S. Shinde, R.J. Deokate, C.H. Bhosale, B.K. Chougule, K.Y. Rajpure, Appl. Surf. Sci. 255 (2009) 6675.
[19] A.R. Babar, S.S. Shinde, A.V. Moholkar, K.Y. Rajpure, J. Alloys Compd. 505 (2010) 743.
[20] A.R. Babar, S.S. Shinde, A.V. Moholkar, C.H. Bhosale, J.H. Kim, K.Y. Rajpure, J. Alloys Compd. 505 (2010) 416.
[21] S.S. Shinde, P.S. Patil, R.S. Gaikwad, R.S. Mane, B.N. Pawar, K.Y. Rajpure, J. Alloys Compd. 503 (2010) 416.
[22] K.K. Patankar, S.S. Joshi, B.K. Chougule, Phys. Lett. A 346 (2005) 337.
[23] D.K. Pradhan, B.K. Samantary, R.N.P. Chaudhary, A.K. Thakur, Mater. Sci. Eng. B 116 (2005) 7.
[24] J. Wang, F.Q. Wu, G. Song, N. Wu, J.P. Wang, Ferroelectrics 323 (2005) 71.
[25] J.R. Macdonald, Impedance Spectroscopy, Wiley, New York, 1987.
[26] G.E. Youngblood, R.W. Rice, R.P. Ingel, J. Am. Ceram. Soc. 71 (1988) 255.
[27] S.S. Shinde, K.Y. Rajpure, J. Solid State Chem. 183 (2010) 2886.
[28] P.G. Klemens, Physica B 263 (1999) 102.